The crystal-fluid interfacial free energy and nucleation rate of NaCl from different simulation methods

Jorge R. Espinosa, Carlos Vega, Chantal Valeriani, and Eduardo Sanz

Citation: The Journal of Chemical Physics **142**, 194709 (2015); doi: 10.1063/1.4921185
View online: http://dx.doi.org/10.1063/1.4921185
View Table of Contents: http://scitation.aip.org/content/aip/journal/jcp/142/19?ver=pdfcov
Published by the AIP Publishing

The crystal-fluid interfacial free energy and nucleation rate of NaCl from different simulation methods

Jorge R. Espinosa, Carlos Vega, Chantal Valeriani, and Eduardo Sanz
Departamento de Química Física, Facultad de Ciencias Químicas, Universidad Complutense de Madrid, 28040 Madrid, Spain

(Received 13 February 2015; accepted 4 May 2015; published online 21 May 2015)

In this work, we calculate the crystal-fluid interfacial free energy, γ_{cf}, for the Tosi-Fumi model of NaCl using three different simulation techniques: seeding, umbrella sampling, and mold integration. The three techniques give an orientationaly averaged γ_{cf} of about 100 mJ/m^2. Moreover, we observe that the shape of crystalline clusters embedded in the supercooled fluid is spherical. Using the mold integration technique, we compute γ_{cf} for four different crystal orientations. The obtained interfacial free energies range from 100 to 114 mJ/m^2, being (100) and (111) the crystal planes with the lowest and highest γ_{cf}, respectively. Within the accuracy of our calculations, the interfacial free energy either does not depend on temperature or changes very smoothly with it. Combining the seeding technique with classical nucleation theory, we also estimate nucleation free energy barriers and nucleation rates for a wide temperature range (800-1040 K). The obtained results compare quite well with brute force calculations and with previous results obtained with umbrella sampling [Valeriani *et al.*, J. Chem. Phys, **122**, 194501 (2005)]. © *2015 AIP Publishing LLC.* [http://dx.doi.org/10.1063/1.4921185]

I. INTRODUCTION

The crystal-fluid interfacial free energy, γ_{cf}, is a crucial parameter in crystal nucleation and growth, as well as in wetting phenomena.[1–3] Unfortunately, it is quite difficult to measure γ_{cf} experimentally.[4] Typically, experimental measurements of the crystal nucleation rate are combined with Classical Nucleation Theory (CNT)[3] to estimate both the height of the nucleation barrier and the interfacial free energy.[5–8]

Computer simulations are a useful tool to estimate crystal-fluid interfacial free energies. Several simulation methods have been implemented for that purpose: the cleaving method,[9] the capillary fluctuation technique,[10] metadynamics,[11,12] tethered Monte Carlo (MC),[13] the contact angle approach,[14,15] the seeding method,[16–18] umbrella sampling (US),[19] and the mold integration (MI) technique.[20] For systems like Lennard Jones,[12,20–22] hard spheres,[13,20,23–25] or water,[17,18,26–28] some of these techniques have been used by different groups and a reasonable consensus on γ_{cf} has been reached. However, this is not the case for sodium chloride.

In 2005, two different values of γ_{cf} for the Tosi-Fumi model[29,30] of NaCl were reported: 36 mJ/m^2, based on measures of the contact angle of a liquid drop on top of its solid;[14,31] and 99 mJ/m^2, based on calculations of the nucleation free energy barrier combined with classical nucleation theory.[32] These discrepancies were ascribed to finite size effects in small crystal clusters in a combined effort by both groups later on in 2008.[33]

In our present work, we calculate γ_{cf} for the Tosi-Fumi NaCl model by three different techniques, namely, mold integration, seeding, and umbrella sampling. The MI method consists in calculating the work needed to reversibly induce the formation of a crystal slab in the fluid under coexistence conditions. The seeding technique consists in inserting large crystalline clusters in the supercooled fluid and determining the temperature at which such clusters are critical. Then, CNT is used to provide estimates of the interfacial free energy. By means of the US method, it is possible to compute the free energy needed to form crystal clusters and then CNT is used to derive the interfacial free energy. Contrary to both umbrella sampling and seeding methods, the mold integration technique does not rely on CNT and provides direct measures of γ_{cf}.

We find that the three techniques give a γ_{cf} averaged over crystal orientations of about 100 mJ/m^2. This good agreement is obtained assuming a spherical shape for the clusters both in seeding and in umbrella sampling. This assumption is justified by our analysis of the shape of the clusters in the seeding technique that confirms their spherical shape. The seeding technique also allows us to evaluate the dependence of γ_{cf} with temperature and to conclude that γ_{cf} does not depend on temperature.

The nucleation rate, i.e., the number of clusters formed per unit of time and volume, is even more relevant to characterise the process of crystal nucleation than the interfacial free energy. Contrary to γ_{cf}, the nucleation rate can be directly measured experimentally.[34–36] By means of our seeding simulations, CNT, and calculations of the attachment rate of particles to the critical cluster, we estimate the nucleation rate and find a good agreement between numerical simulations and experiments.

II. NaCl MODEL

Several model potentials have been implemented to simulate alkali halides such as those proposed by Smith and Dang,[37] by Joung and Cheatham,[38] or by Tosi and Fumi.[29,30] We opt for the Tosi-Fumi potential, whose properties are quite close to those of real NaCl,[29,30,39] in order to be able to compare

TABLE I. Parameters for the Tosi-Fumi NaCl,[29] A_{ij} in kJ/mol, B in Å^{-1}, C_{ij} in Å^6 kJ/mol, D_{ij} in Å^8 kJ/mol, and σ_{ij} in Å.

	A_{ij}	B	C_{ij}	D_{ij}	σ_{ij}
Na–Na	25.4435	3.1546	101.1719	48.1771	2.340
Na–Cl	20.3548	3.1546	674.4793	837.0770	2.755
Cl–Cl	15.2661	3.1546	6985.6786	14 031.5785	3.170

with previous studies.[14,31,32] Tosi-Fumi[29] is a two-body and non-polarizable potential,

$$U(r_{ij}) = A_{ij}e^{B(\sigma_{ij}-r_{ij})} - \frac{C_{ij}}{r_{ij}^6} - \frac{D_{ij}}{r_{ij}^8} + \frac{q_i q_j}{r_{ij}}, \qquad (1)$$

where r_{ij} is the distance between two ions with charge $q_{i,j}$. The first term is the Born-Mayer repulsive term, $-\frac{C_{ij}}{r_{ij}^6}$ and $-\frac{D_{ij}}{r_{ij}^8}$ are the van der Waals attractive interaction terms, and the last one corresponds to the Coulomb interaction. The parameters A_{ij}, B, C_{ij}, D_{ij}, and σ_{ij} are given in Table I.

In this work, we have truncated the non-Coulomb part of the potential at $r_c = 14$ Å and added long range tail corrections to the energy (when simulating the system with MC and Molecular Dynamics (MD)) and pressure (in MD). We have used Ewald sums (in MC) to deal with Coulomb interactions, truncating the real part of the sums at the same cut-off. For MD calculations, we have used PME (Particle-Mesh Ewald method)[40] truncating at the same cut-off.

III. SIMULATION DETAILS

We have used the GROMACS 4.5.5 package[41,42] to perform molecular dynamics simulations in the NpT ensemble. The Tosi-Fumi NaCl potential has been implemented in GROMACS in a tabulated form. The time step for the velocity-Verlet algorithm was set to 0.002 ps and a velocity-rescale thermostat with a relaxation time of 0.5 ps was used to keep constant the selected temperature.[43] All our simulations are carried out at 1 bar using the Parrinello-Rahman barostat[44] with a relaxation time of 0.5 ps.

IV. MOLD INTEGRATION METHOD

This methodology has been recently proposed by Espinosa *et al.*[20] and allows to calculate the crystal-fluid interfacial free energy for a flat interface (at coexistence). The method has been validated with the calculation of γ_{cf} for hard spheres and Lennard-Jones.[20]

The basic idea of this methodology is to reversibly induce the formation of a thin crystalline slab in the fluid with the aid of a mold of potential energy wells placed in the sites of a lattice plane. By switching on a square-well-like interaction between the wells and the fluid particles, the latter remain confined in the mold inducing the appearance of a thin crystal slab as sketched in Fig. 1.[45] In Fig. 1(a), the mold (orange and gray spheres) is switched off and the fluid (small particles) does not feel its presence. In (b), the mold is switched on and each well is filled with a fluid particle, which creates a crystal slab around the mold. The work needed to go from (a) to (b) is related to the work required to create two crystal-fluid interfaces.[20]

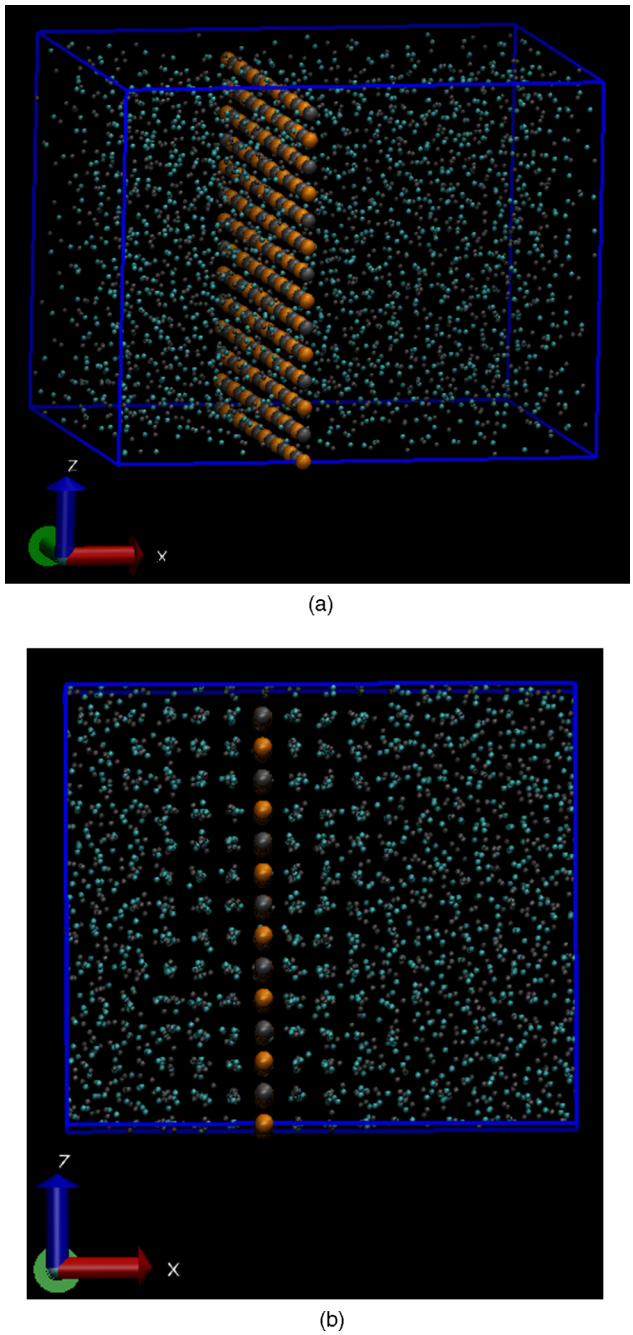

FIG. 1. Top: Snapshot of a sodium chloride fluid at coexistence (green and black ions). Bottom: Snapshot of a fluid with a thin crystal slab at coexistence conditions. The diameter of the ions has been reduced to 1/4 of its original size. The mold that induces the formation of the crystal slab is conformed by a set of potential energy wells (in orange the ones for sodium ions and in grey the ones for chloride ions) whose positions are given by the lattice sites of the selected crystal plane, (100) in this case, at coexistence conditions. The interaction between the mold and the ions is switched off in (a) and on in (b).

The only difference from the present work and Ref. 20 in terms of methodology is that here we use two different types of wells that selectively attract either Na^+ or Cl^- ions. (The systems studied in Ref. 20 were mono-component, so every well interacted with every particle.) In Sec. IV A, we describe how the interfacial free energy is calculated for the

(100) plane of NaCl with the MI method and give the results for other orientations.

A. Calculation of γ_{cf} with the MI method

In this section, we report the calculation of γ_{cf} for four different crystal orientations using the MI method. We will start with explaining in more detail the calculations for the 100 plane and then give the results for all other orientations.

The first step is obtaining the mold coordinates and a fluid configuration at coexistence conditions. The dimensions of the mold have to be coherent with the unit cell parameters at coexistence conditions. In Figs. 1 and 2, we show a representation of the molds used to induce the appearance of different crystal-fluid interfaces.

The mold for the (100) orientation has 196 wells, half for sodium and half for chloride ions. The fluid consists of 2744 ions equilibrated at coexistence conditions. The simulation box where the fluid is equilibrated is prepared in such way that the area of one of its sides coincides with that of the mold (see Fig. 1(a)). This side is kept fixed and to maintain the pressure constant, variations of the volume are made through changes in the direction perpendicular to it, which in our case is the x direction (we refer to this type of simulations as Np_xT[46]). The mold is kept fixed throughout the simulation.

Once a fluid-mold configuration is prepared, we need to find the potential well radius that gives the correct value for γ_{cf}, r_w^o (the work needed to fill the mold depends on the well radius and there is only one radius for which the correct interfacial free energy is obtained[20]). To find r_w^o, we run, for different values r_w of the well radius, several Np_xT trajectories starting from a fluid configuration where we switch on the mold at the beginning of the simulation. In the present paper, we launch 8 trajectories of 1 ns for each r_w. We set the depth of the square-well-like interaction between wells and particles to $\epsilon_m = 7.5\ k_BT$. This ensures that the mold is permanently filled (195.6 out of 196 wells are filled on average). Along each trajectory, we monitor a parameter that accounts for the global degree of crystallinity, ξ,

$$\xi = \frac{\rho - \rho_f}{\rho_s - \rho_f}, \tag{2}$$

where ρ is the actual density of the system, and ρ_f and ρ_s are the coexistence densities of the fluid and the solid, respectively. Therefore, ξ fluctuates around 0 when the whole system is fluid and around 1 when is crystalline. As a crystal slab grows in the fluid, ξ takes intermediate values. This is just a simple way to quantify the crystallinity degree, but one can also use a method based on counting the number of ions in the largest cluster of solid-like ions, using the same local order parameter as the one we use in the "seeding" technique (see below). By means of the trajectories launched for each r_w, we obtain a probability distribution $P(\xi)$ needed to estimate the free energy profile associated to the order parameter ξ,

$$G(\xi)/(k_BT) = -\ln P(\xi) + constant. \tag{3}$$

The constant is not known, but we are interested in whether the free energy profile shows a minimum or not. As discussed in Ref. 20, if r_w is too large, the system is in the free energy basin corresponding to the fluid, as the mold is not able to induce the formation of a stable crystal slab. If, on the contrary, r_w is too small, the mold provides more energy than that required for the formation of the crystal slab and the $G(\xi)$ profile does not show a basin (a minimum) corresponding to the fluid phase. Accordingly, the free energy profile where the minimum first disappears gives r_w^o. In Fig. 3, we represent the free energy profiles for four different values of r_w.

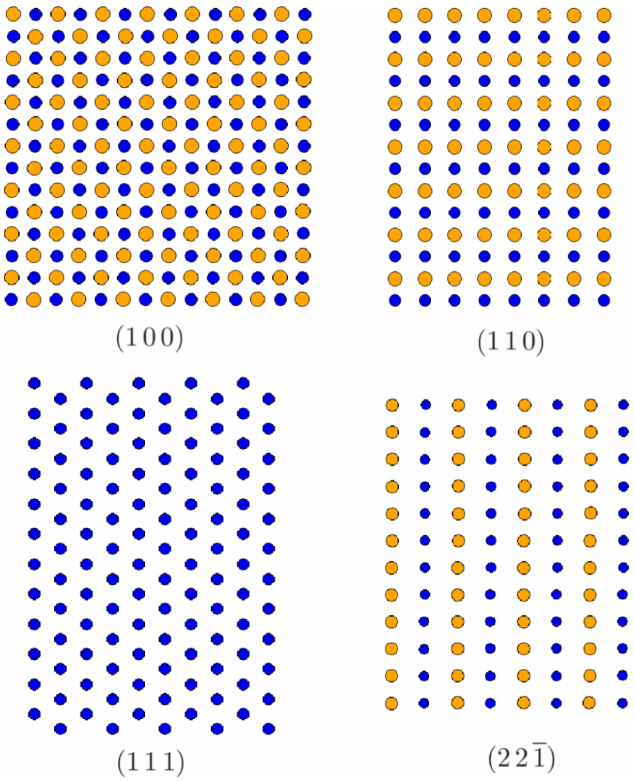

FIG. 2. Molds used to induce the formation of crystal slabs for the different crystal orientations.

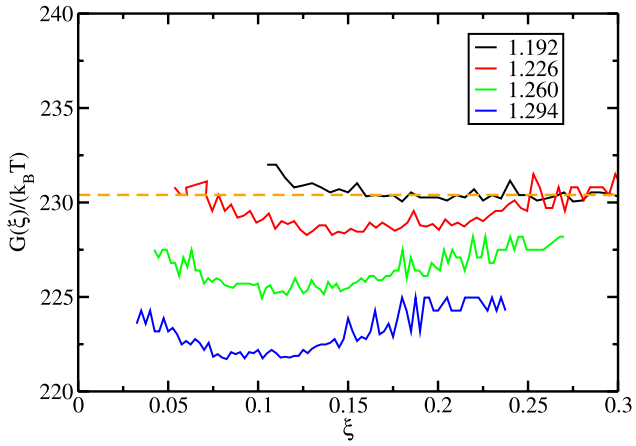

FIG. 3. Free energy profile as a function of the crystallinity degree, ξ, for the 100 plane and for different well radii as indicated in the legend (in Å). In order to compare all curves in the same scale, we have shifted each minimum to the work needed to fill the mold for the corresponding well radius (calculated via thermodynamic integration). For the case where the minimum is absent (black curve), we have shifted the plateau to the work needed to fill a mold of wells with $r_w = r_w^o$, given by the dashed horizontal line.

$G(\xi)$ for r_w = 1.294, 1.260, and 1.226 Å clearly shows a minimum whereas for r_w = 1.192 Å it does not. Therefore, $r_w^o \in [1.192, 1.226$ Å$]$. Taking the mid point of the interval, r_w^o = 1.21 Å. The statistics of the free energy given by Eq. (3) is reasonably good only when the system repeatedly samples configurations in the vicinity of a free energy minimum. Therefore, the use of Eq. (3) must be restricted to small values of crystallinity. An alternative approach to determine r_w^o, based on the inspection of $\xi(t)$ for various trajectories, is discussed in Ref. 20.

Once r_w^0 is obtained, the next step is to calculate $\gamma_{cf}(r_w)$ for $r_w > r_w^0$ by means of thermodynamic integration (thermodynamic integration can only be performed for $r_w > r_w^0$, where the system is still in the fluid basin and the integration is reversible[20]),

$$\gamma_{cf}(r_w) = \frac{1}{2A}\left(\epsilon_m N_w - \int_0^{\epsilon_m} d\epsilon \langle N_{fw}\rangle\right), \qquad (4)$$

where ϵ is the well depth and ϵ_m is the maximum well depth, A is the area of the interface (or the area of the mold), N_w is the total number of wells, and N_{fw} is the number of filled wells. To calculate the integral in Eq. (4), Np_xT simulations are performed for several well depths between $\epsilon = 0$ and $\epsilon = \epsilon_m$. The average number of filled wells ($\langle N_{fw}\rangle$) is computed in each simulation. In Fig. 4, we plot $\langle N_{fw}\rangle$ versus ϵ for r_w = 1.26 Å.

Beyond $\epsilon \approx 5\ k_BT$, all wells are almost permanently filled. Note that the result of Eq. (4) does not depend on the value of ϵ_m as long as all wells are filled when $\epsilon = \epsilon_m$. Therefore, to avoid performing useless calculations, it is not convenient that ϵ_m largely exceeds the value of ϵ beyond which the wells are permanently filled. By integrating the curve shown in Fig. 4, we obtain $\gamma_{cf}(r_w = 1.26$ Å$) = 97.5$ mJ/m^2. We made sure that the integration was reversible by switching off the mold at the end of the calculation and checking that the crystallinity degree ξ readily goes to 0 for all values of ϵ. The closer r_w to r_w^o the shallower the fluid basin and the more likely the integration is not reversible. Therefore, large values of r_w are preferred in this respect. However, one cannot increase r_w beyond the point where more than one particle

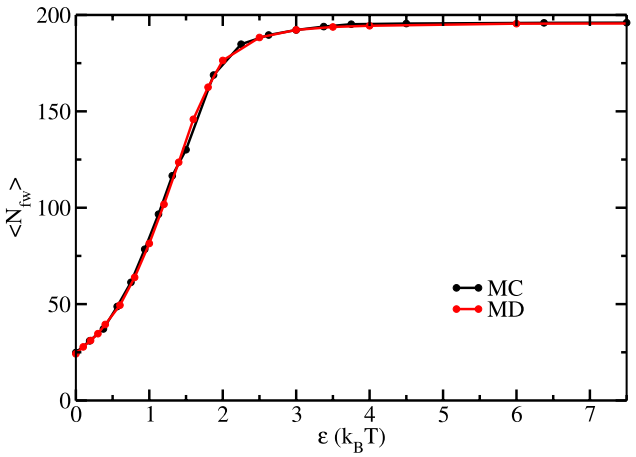

FIG. 4. Average number of filled wells, $\langle N_{fw}\rangle$, as a function of the depth of the well, ϵ. The plot corresponds to the (100) face and to a 196-well mold with r_w = 1.26 Å. The red and black curves correspond to MD and MC simulations, respectively.

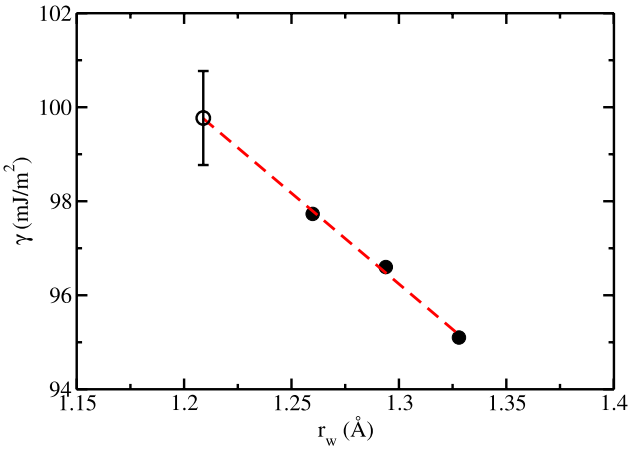

FIG. 5. The solid filled symbols represent the interfacial free energy versus the potential well radius for the (100) plane. The red dashed line is a linear fit to the solid symbols. The empty symbol is an extrapolation of the fit to r_w^o, that gives our estimate for the interfacial free energy.

fits in each well. As we show in Fig. 4, the simulations can be either performed with a bespoke MC code or with an MD package, such as GROMACS (in Ref. 20, some hints on how to implement the MI method in GROMACS are given). MD simulations to obtain each of the points in Fig. 4 are 800 ps long (50 ps for equilibration and 750 for production) and MC are 100 000 cycles (10 000 for equilibration and 90 000 for production).

The calculations described in the previous paragraph for r_w = 1.26 Å are repeated for several $r_w > r_w^o$ in order to obtain a $\gamma_{cf}(r_w)$ curve that can then be extrapolated to r_w^o (shown in Fig. 5).

By performing a linear extrapolation to r_w^o, we obtain a γ_{cf} for the 100 crystal plane of (100 ± 1) mJ/m^2. Using the molds shown in Fig. 2, we repeat the same calculation for other crystal orientations. In Table II, we report, for each orientation, the system size, the number of wells, the optimal radius, and the calculated γ_{cf}.

All crystal planes have a γ_{cf} of about 100 mJ/m^2 except the (111) plane, whose γ_{cf} is 15% higher. This is perhaps not totally unexpected since the (111) plane, contrary to all other planes, is constituted of ions of the same chemical identity, therefore it is not electro-neutral. In principle, one could suspect that the (111) interface is unstable because of the dipolar moment coming from the stacking of charged planes parallel to the interface.[47] However, this dipolar interaction can be efficiently screened by the melt, a dense fluid of charged particles. In fact, it has been recently shown that the 111

TABLE II. Interfacial area ($L_y \times L_z$), number of wells (N_w), number of particles (N_{Tot}), optimal well radius (r_w^o), and interfacial free energy (γ_{cf}) for all crystal orientations studied with the MI method.

hkl	$(L_y \times L_z)$ (Å^2)	N_w	N_{Tot}	r_w^o (Å)	γ_{cf} ($\frac{\text{mJ}}{\text{m}^2}$)
(100)	41.40×41.40	196	2744	1.21	100 ± 1
(110)	33.45×41.40	112	2688	1.07	103 ± 1
(111)	36.21×50.18	120	2880	0.87	114 ± 1
(22$\bar{1}$)	36.21×40.97	120	2880	1.07	105 ± 1

crystal-melt interface of NaCl is rough and shows no signs of being unstable or undergoing surface reconstruction.[48]

V. SEEDING

A. The seeding technique

This technique has been first proposed by Bai and Li[16,49] for the calculation of the crystal-fluid interfacial free energy of the Lennard-Jones system. Later on, it was used to determine γ_{cf} for clathrates[17] and for several water models.[18,28] In brief, it consists in inserting a crystalline cluster in a supercooled fluid and performing simulations at several temperatures while monitoring the size of the cluster. If the chosen temperature is below the temperature at which the cluster is critical, the cluster will grow, whereas if it is above, the cluster will melt. So the temperature at which the cluster is critical is enclosed in between the highest temperature at which the cluster grows and the lowest at which it melts. This approach is similar to the one used by Pereyra *et al.*[50] to determine the temperature at which a cylindrical crystalline slab of ice melts or grows.

Once the temperature at which the cluster is critical is known, the seeding approach makes use of CNT to obtain estimates of the interfacial free energy. According to CNT,[3] the free energy required for the formation of a crystalline cluster in the supercooled fluid is

$$\Delta G(N) = -N|\Delta\mu| + A\gamma_{cf}, \tag{5}$$

where $\Delta\mu$ is the chemical potential difference between the crystal and the supercooled fluid, N is the number of particles in the crystal cluster, and A is the cluster's surface area. Assuming that the crystalline cluster has a spherical shape, the value of N that maximizes ΔG (N_c) is given by

$$N_c = \frac{32\pi\gamma_{cf}^3}{3\rho_s^2|\Delta\mu|^3}, \tag{6}$$

where ρ_s is the density of the solid phase. This equation allows to estimate γ_{cf}. There are two ways of calculating $\Delta\mu$. The first one is by means of thermodynamic integration from the coexistence temperature, where $\Delta\mu = 0$. The other is by approximating $\Delta\mu$ by $\Delta H_m(1 - T/T_m)$, where ΔH_m is the melting enthalpy and T_m is the melting temperature. We have checked that the approximation works well and gives the same result as the rigorous thermodynamic integration.

Apart from obtaining estimates of γ_{cf} via Eq. (6), one can estimate the nucleation free energy barrier (ΔG_c) and the nucleation rate (J) with CNT. The free energy barrier for nucleation is given by

$$\Delta G_c = \frac{N_c}{2}|\Delta\mu|. \tag{7}$$

Following the approach described by Auer and Frenkel,[3,19,51] the nucleation rate J can be obtained from the expression,

$$J = \rho_f Z f^+ \exp(-\Delta G_c/(k_B T_c)), \tag{8}$$

where the product $\rho_f Z f^+$ defines the kinetic prefactor, κ_p, where f^+ the attachment rate of particles to the critical cluster, ρ_f the fluid density, and Z the Zeldovich factor.[3] The CNT form of the Zeldovich factor is

$$Z = \sqrt{(|\Delta G''|_{N_c}/(2\pi k_B T_c))} = \sqrt{|\Delta\mu|/(6\pi k_B T_c N_c)} \tag{9}$$

so that Z can be computed once the size of the critical cluster, N_c, the temperature at which it is critical, T_c, and the chemical potential difference between the solid and the liquid are known. According to Refs. 19, 32, and 51, f^+ can be computed as a diffusion coefficient of the cluster size at the top of the barrier (which requires launching about 10 runs at the temperature at which the cluster is critical),

$$f^+ = \frac{\langle (N(t) - N_c)^2 \rangle}{2t}. \tag{10}$$

Alternatively, f^+ can be approximated in a way that does not require running simulations of the critical cluster.[3] According to Ref. 3, since the attachment rate f^+ is related to the time required for a particle to attach to the crystal cluster, it can be estimated as

$$f^+ = \frac{24D(N_c)^{2/3}}{\lambda^2}, \tag{11}$$

where λ^2/D is the time needed for a molecule to diffuse the typical distance (λ) required to attach to the cluster and D is the diffusion coefficient of the supercooled liquid.

The seeding technique can be particularly useful at low and moderate supercooling, where estimating the critical cluster size, the free-energy barrier height and the rate by more rigorous numerical techniques would be very expensive (from a computational point of view).

B. Approximations in the seeding approach

The seeding technique is an approximate approach to calculate γ_{cf}. First of all, it relies on the validity of CNT. Next, the inserted clusters have a defined shape. The expressions above for the CNT correspond to the assumption that the clusters are spherical. We will discuss later on that this is actually a good approximation for NaCl. The interfacial free energy thus obtained corresponds to an average over all possible crystal orientations, so the technique does not provide information about the anisotropy of γ_{cf} with the orientation of the crystal. Finally, the method heavily relies on the way the number of particles in the cluster (N_c) is determined. This is typically evaluated with the aid of local bond-order parameter, which is able to discriminate between liquid-like and solid-like particles.[52] Therefore, N_c depends on the specific choice of the order parameter. Of course, reasonable choices of order parameter give similar values for N_c, but differences of about 30% in the number of particles can be found between different order parameters. According to Eq. (6), a 30% error in N_c results in an uncertainty of 10% in γ_{cf}. Therefore, the ambiguity in the determination of N_c substantially affects the accuracy with which γ_{cf} is determined via the seeding technique.

In this work, we use the same order parameter as in Ref. 32 to measure N_c. In Ref. 32, the order parameter was tuned so that the percentage of particles wrongly labelled as liquid-like in the bulk solid was the same as that of particles wrongly labelled as solid-like in the bulk liquid. The same criterion was

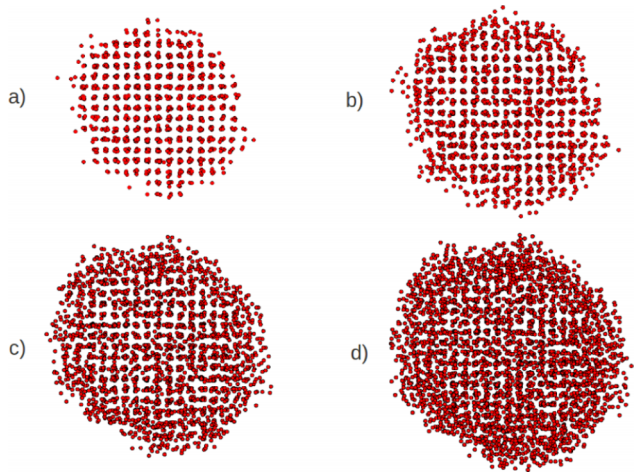

FIG. 6. (a) Snapshot of a solid cluster as detected by the local order parameter used in this work (same as in Ref. 32). (b) Same cluster as in (a) but with an extra layer of particles attached to it. (c) Same cluster as in (a) but with two extra layers of particles attached to it. (d) Same cluster as in (a) but with three extra layers of particles attached to it. The crystalline character of the cluster fades as extra layers are added.

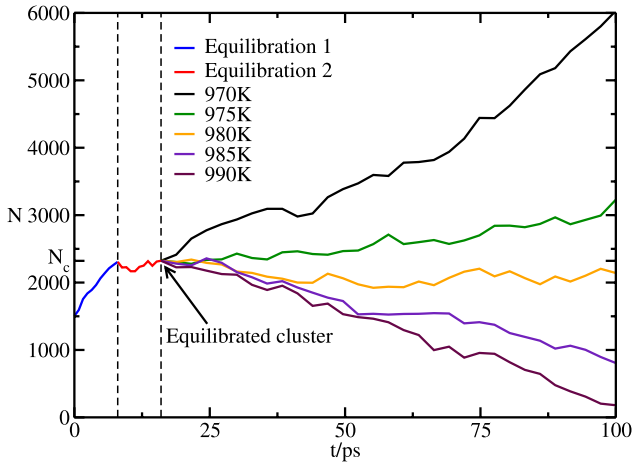

FIG. 7. Number of particles in the cluster (N) versus time. During the first stage of equilibration (8 ps, blue curve) the cluster is kept frozen and it grows as the interface equilibrates. In the second stage (red curve) the constraint is released and the system is equilibrated for another 8 ps. These two equilibration runs are performed at 925 K. Finally, several simulations starting from the configuration of the equilibrated cluster are run at different temperatures to locate the temperature at which such cluster is critical.

used to tune the order parameter when studying the ice-water interface and this led to reasonable values for γ_{cf}.[18,28]

We can also check if our choice of the order parameter is reasonable by visually inspecting the clusters.

In Fig. 6(a), we show the top view of a cluster as detected by our order parameter. The crystalline features of the cluster can be clearly appreciated. In Figs. 6(b)–6(d), we show the snapshots resulting from adding 1, 2, and 3 extra layers of particles to the cluster originally detected by our order parameter. These extra layers do not perfectly fit on top of the underlying solid lattice. Therefore, the order parameter employed seems to be a good one because it does not add a fluid-like layer to the cluster (neither removes a solid-like layer from it).

C. Setup for the seeding technique

To prepare the initial configuration, we insert a crystalline cluster in the supercooled fluid and remove the fluid molecules that overlap with the cluster. Then, the fluid-crystal interface is equilibrated for 8 ps keeping the positions of the ions of the inserted cluster fixed. In this way, the cluster does not loose particles and the interface is equilibrated by the attachment of new particles to the cluster. Then, the constraint is released and the system is further equilibrated for 8 ps until N varies smoothly with time. Following equilibration, we launch trajectories at different temperatures to find the temperature at which the equilibrated cluster is critical.

In Fig. 7, we show the evolution of N with time during equilibration and during production, when trajectories are launched at different temperatures from the equilibrated cluster. The equilibration is typically performed at low temperatures (925 K in this particular case) to avoid the cluster loosing particles during the second stage of equilibration.

A list of all cluster sizes after equilibration is given in Table III.

In each system, the total number of ions is approximately 20 times larger than the inserted cluster to avoid interactions between the cluster and its periodic images. The total number of ions, N_{Tot}, for each system (considering the solid cluster and the supercooled fluid) is also given in Table III: in order to be able to simulate such large systems, we had to recur to supercomputing facilities.

D. Cluster shape

The CNT expressions given above correspond to the assumption that the critical cluster adopts a spherical shape. In principle, this is a reasonable assumption because a sphere is the shape with the lowest surface area. However, in Ref. 32, it was suggested that the cluster could be cubic rather than spherical. This is a plausible possibility for the cluster's shape, given that NaCl has a cubic unit cell. To investigate if the shape of the cluster is spherical or cubic, we equilibrate both a cubic cluster and a spherical cluster and compare the shape of the resulting clusters. In Fig. 8(a), we show a snapshot of both clusters just after being inserted and in Fig. 8(b) after the equilibration of the interface.

In Fig. 8(b), 60 independent equilibrated clusters are superimposed (with the same orientation) in order to get a

TABLE III. Number of ions in the critical cluster (N_c), total number of ions in the system (N_{Tot}), temperature at which the cluster is found to be critical (T_c [K]), density of the solid at that temperature (ρ_s [g/cm^3]) and the interfacial free energy from Eq. (6) in mJ/m^2.

N_c	N_{Tot}	T_c	ρ_s	γ_{cf}
284	21 724	857.5	1.95	113
1 152	46 522	962.5	1.92	97
2 322	46 396	980.0	1.91	104
8 084	110 248	1007.5	1.90	114
11 164	194 920	1022.5	1.89	102

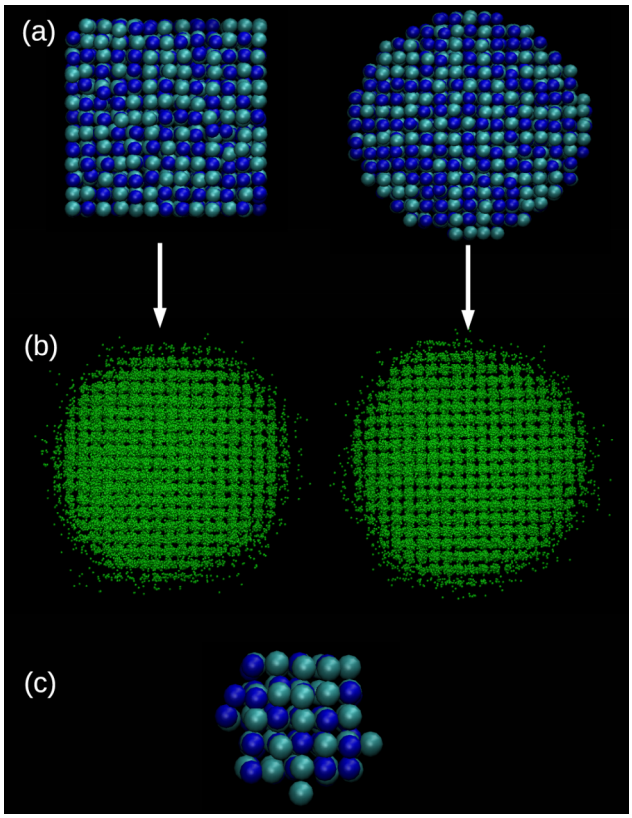

FIG. 8. Snapshots of different crystalline NaCl clusters. (a) A cubic (left) and a spherical (right) cluster of about 2000 particles obtained from the bulk solid lattice. (b) A superimposition of 60 clusters equilibrated as described in the main text from the clusters in (a). (c) A sphere of 130 particles obtained from the bulk solid lattice. The shape of the cluster looks cubic rather than spherical due to the limited number of particles.

statistical representation of the average cluster shape. Both equilibrated clusters have a very similar average shape that clearly looks more spherical than cubic. Some faceting is present that makes the average shape different from that of a perfect sphere. But such faceting is also present in the spherical cluster originally inserted (Fig. 8(a), right) and is a consequence of discretizing a sphere with a cubic lattice. To quantify the degree of sphericity of the clusters, we expanded their density with respect to their center of mass in rank four spherical harmonics and calculated the quadratic invariant S_4.[53] The 60 clusters equilibrated from a sphere give an average S_4 of 0.03 while those coming from a cube give $S_4 = 0.034$. S_4 for a perfect sphere is 0.003 and for a perfect cube 0.115. Therefore, both cubic and spherical clusters equilibrate to a shape which is closer to a sphere. In summary, we can consider our clusters spherical and confidently use the CNT expressions above.

E. Interfacial free energy

Once the cluster is equilibrated, we perform MD runs at different temperatures and monitor the cluster size to determine the temperature at which each cluster is critical, as shown in Fig. 7 for one of the clusters. In the example of Fig. 7, the size of the cluster does not change during the simulation at T = 980 K, so we consider this as the temperature at which a cluster with $N_c = 2322$ particles is critical. Once we know T_c, we obtain $\Delta\mu$ as $\Delta H_m(1 - T_c/T_m)$. Next, we measure in an NpT simulation ρ_s at T_c: in this way, we obtain all variables needed to obtain γ_{cf} via Eq. (6). For this model, $\Delta H_m = 3.36$ kcal/(mol of ions) and $T_m = 1082$ K.[39] The results obtained for all clusters are reported in Table III.

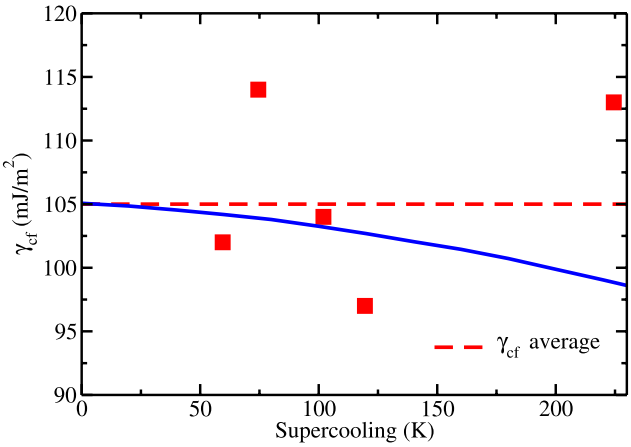

FIG. 9. Interfacial free energy estimated via Eq. (6) for the critical clusters studied as a function of the supercooling. Within the accuracy of our data, γ_{cf} does not change with the supercooling. The dashed line is the average γ_{cf} and the solid line is the variation of γ_{cf} with temperature predicted by Turnbull.

In Fig. 9, we show that, within the accuracy of our data, the interfacial free energy does not change with the supercooling (the difference between the melting temperature and the temperature of interest). This implies, according to the thermodynamic relation $-S_{cf} = (\partial\gamma_{cf}/\partial T)_p$, that the entropic cost of forming the crystal-fluid interface for NaCl is either zero or very small. In Fig. 9, we also show the $\gamma(T)$ dependence predicted by Turnbull's rule[54] ($\gamma_{cf} = C_T\rho_s^{2/3}\Delta H(T)/N_A$, where N_A is Avogadro's number, $\Delta H(T)$ is the enthalpy difference between the liquid and the solid, and $C_T = 0.394$ is the Turnbull's constant obtained from the calculated γ_{cf} at coexistence (105 mJ/m^2)). Turnbull's rule has been successfully used to predict nucleation times for Al and Lennard-Jones systems.[55,56] The mild decrease of γ as the supercooling increases predicted by Turnbull is consistent with our data. Since our data do not show a clear temperature dependence, we obtain γ_{cf} at the melting temperature simply by averaging γ_{cf} for all supercoolings studied. This average is indicated in Fig. 9 with a dashed line and corresponds to 105 mJ/m^2. As discussed above, this value is subject to a systematic error of about 10% due to the arbitrariness of the order parameter. The statistical error of the determination of T_c in our simulations raises the error in γ_{cf} up to 20%.

F. Free energy barriers and nucleation rates

Once the interfacial free energy is calculated, we can obtain ΔG_c, the work needed to form a critical cluster in the metastable fluid, via Eq. (7). Then, we compute the attachment rate via Eq. (10) to finally obtain the nucleation rate from Eq. (8). To calculate the attachment rate via Eq. (10), we launch 10 trajectories at T_c from the equilibrated cluster (with N_c particles) and monitor N to obtain an average curve of $(N(t) - N_c)^2$. The slope of such curve, that should be a straight

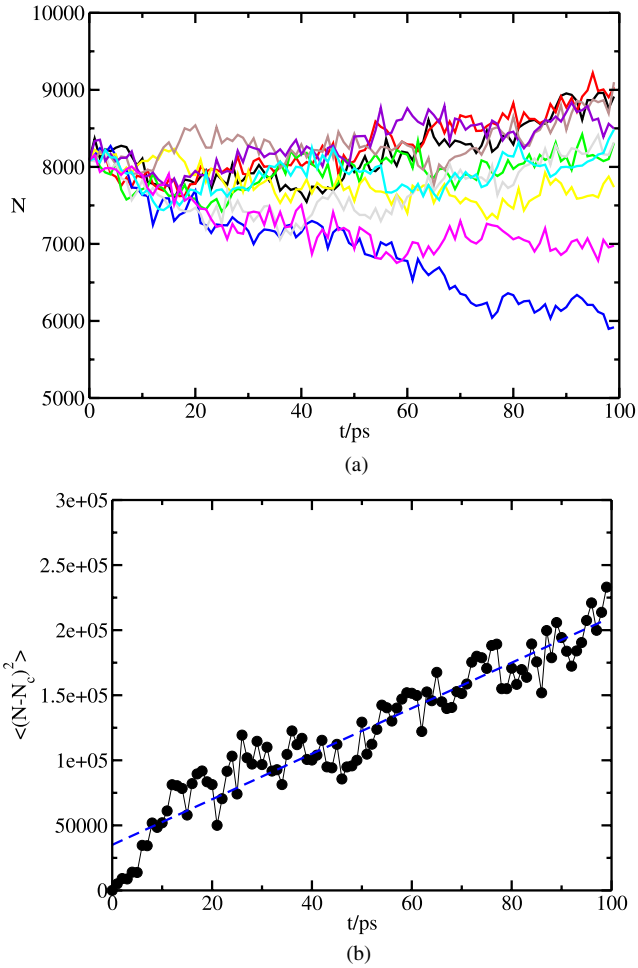

FIG. 10. (a) N versus time for 10 trajectories launched at the temperature at which the cluster is critical ($T = 1007.5$ K). (b) $\langle (N - N_c)^2 \rangle$ versus time, whose slope is related to the attachment rate by Eq. (10).

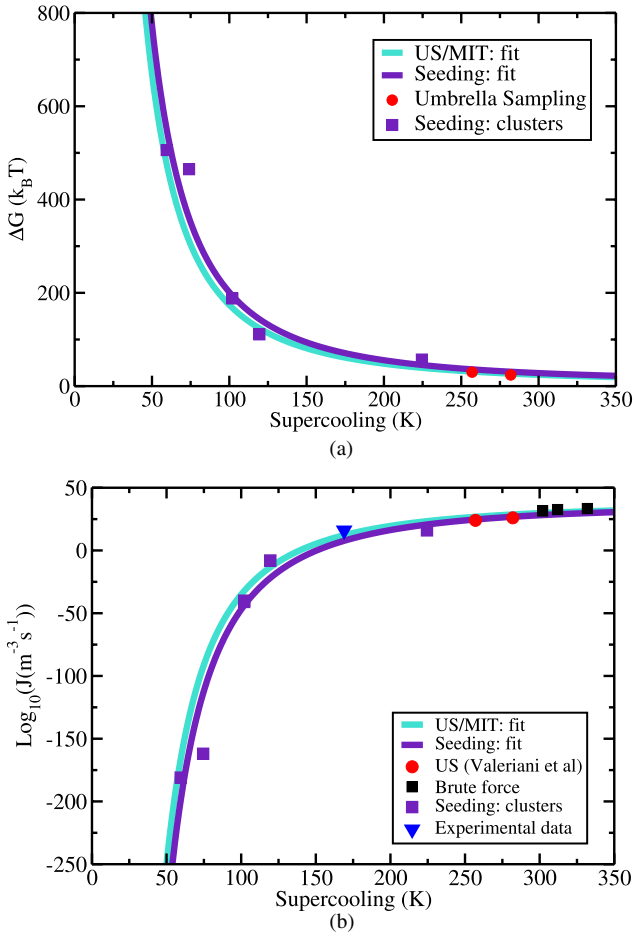

FIG. 11. Free energy barrier height, (a), and nucleation rate, (b), as a function of the supercooling. Purple squares correspond to our seeding data, red circles are results from Ref. 32, the blue triangle is an experimental data from Refs. 34–36, and the black squares are our calculations of the nucleation rate from brute force MD calculations. The curves are fits based on the seeding data (purple) and on the estimates of γ_{cf} at coexistence by means of the MI method and US (cyan).

line in the regime in which the cluster diffuses on top of the barrier, is related to the attachment rate by Eq. (10). The time evolution of N in the ten trajectories and the resulting average $(N(t) - N_c)^2$ curve are shown in Fig. 10.

Note that, since the simulations are performed at T_c, in some of the trajectories the cluster grows, in others it shrinks, and in others it does not change its size. In Table IV, we report our results for all quantities needed for the calculation of the nucleation barrier and the nucleation rate.

TABLE IV. Studied cluster sizes (N_c), temperature at which the clusters are found to be critical (T_c) in K and the corresponding values for the attachment rate (f^+), in s^{-1}; the Zeldovich factor (Z); the kinetic prefactor ($\kappa_p = \rho_f Z f^+$), in m^{-3} s^{-1}; the height of the nucleation free energy barrier (ΔG_c), in $k_B T$; the $\log_{10}$ of the nucleation rate (J) in m^{-3} s^{-1}; and the constant λ in Å.

N_c	T_c	$f^+/10^{14}$	$Z/10^{-3}$	$\kappa_p/10^{40}$	ΔG_c	$\log_{10} J$	λ
284	857.5	1.0	17	2.3	57	16	0.3
1 152	962.5	4.2	5.9	3.1	111	−8	1.7
2 322	980.0	6.0	3.8	3.2	188	−41	2.0
8 084	1007.5	10	1.7	3.4	465	−162	1.1
11 164	1022.5	20	1.3	3.5	506	−180	3.4

In Figs. 11(a) and 11(b), we plot both the free-energy and the nucleation rate. Data represented in square purples are our results from the seeding technique, whereas red dots are data from Ref. 32. Our seeding data have been obtained for milder supercooling than those of Ref. 32, but both data sets seem to be consistent at first sight. In Fig. 11(b), we also include the only available experimental data for the nucleation of NaCl from its melt[34–36] (blue triangle). Remarkably, the experimental data are fully consistent with the predictions of the model.

From our seeding calculations, we can estimate the whole dependence of ΔG_c and J with the supercooling. We use Eqs. (6) and (7) to obtain ΔG_c at any temperature. The density of the solid as a function temperature is calculated by fitting several NpT simulations of the bulk solid. The fit thus obtained is ρ_s (g/cm^3) $= 2.259 - 0.000\,358\,11 \cdot T$ (K). As for the γ_{cf}, since it does not depend on T, we can use the average value of 105 mJ/m^2. This gives the purple curve in Fig. 11(a), that shows a good agreement with the points calculated in Ref. 32 by means of US. As expected, the free-energy barrier rapidly grows as the freezing point is approached (zero supercooling)

and homogeneous nucleation becomes increasingly unlikely. To obtain J as a function of the supercooling, we use Eq. (8). The density of the fluid is obtained via a linear fit of ρ_f versus T that we obtain by performing NpT simulations at several supercoolings. The fit thus obtained is ρ_f (g/cm^3) = 2.007 76 − 0.000 570 2 · T (K). The Zeldovich factor, Z, can be obtained at any temperature by using Eqs. (9) and (6) and assuming again a constant γ_{cf} of 105 mJ/m^2. The attachment rate, f^+, can also be estimated at any temperature with the aid of Eq. (11) using a λ averaged over all clusters (⟨λ⟩ = 1.7 Å), and an Arrhenius-like fit of $D(T)$ based on NpT simulations of the fluid (ln D (m^2/s) = −16.019 − 2886.1/T (K)). It is a good approximation to use an average λ because, as shown in Table IV, λ does not change much with temperature and takes physically meaningful values of the order of one atomic diameter (the distance travelled by particles before attaching to the cluster). The curve of J versus supercooling thus obtained is shown in purple in Fig. 11(b). The agreement with both the simulation of Ref. 32 and the experiment[34–36] is confirmed by the fit. Moreover, the fit works well even at very deep supercoolings, where we have estimated the rate by means of brute force simulations (black squares in Fig. 11(b)). To obtain such rate estimates, we simulate the fluid at a temperature, where the free energy barrier is low and nucleation is likely to happen spontaneously, and wait for the system to crystallize. The nucleation rate is estimated as $1/(\langle t\rangle\langle V\rangle)$, where $\langle V\rangle$ is the average system's volume and $\langle t\rangle$ is the average time the fluid takes to crystallize. To compute $\langle t\rangle$, we perform 10 independent runs from the same initial configuration but with different Maxwellian momenta. The system size was 194 920 ions for both 770 and 780 K and the nucleation time was 0.52 and 3.5 ns, respectively. At 750 K, a system with 21 724 ions was used and the nucleation time was 0.53 ns. In summary, using our seeding results, we have obtained a curve that describes the dependency of the nucleation rate with the supercooling. The curve works well both at moderate supercoolings, where it coincides with experiments and previous simulations, and at deep supercoolings, where it is consistent with brute force simulations. The curve also provides nucleation rates for low supercoolings that have been up to date inaccessible to either simulations or experiments.

VI. UMBRELLA SAMPLING AT COEXISTENCE

US simulations[57] can be used to compute the free energy barrier associated with the formation of a crystal cluster in the supercooled fluid.[58] In Ref. 32, US was used to calculate the free energy barrier for the formation of NaCl crystallites at 800 and 825 K. From the height of the barriers obtained in Ref. 32 and using Eq. (6), γ_{cf} can be obtained. Such estimate requires assuming a particular shape for the critical cluster and can only be performed for temperatures below melting. US can also be used to estimate γ_{cf} at coexistence.[59] To do that, the free energy of formation of a crystal cluster ($\Delta G(N)$) is calculated under coexistence conditions. In this case, $\Delta G(N)$ does not reach a maximum value since $\Delta\mu$ is 0, so γ_{cf} cannot be obtained from the barrier height. However, one can use Eq. (5) with $\Delta\mu = 0$ and, assuming a spherical shape for the cluster, obtain γ_{cf} as follows:

$$\gamma_{cf}(N) = \frac{\Delta G(N)}{(36\pi)^{1/3}}\rho_s^{2/3}N^{-2/3}. \quad (12)$$

Note that this approach relies not only on the assumption on the cluster's shape but also on the order parameter used to determine N.

This approach was followed in Ref. 33 to estimate γ_{cf} at coexistence. The coexistence temperature for the NaCl Tosi-Fumi model has been previously calculated and it ranges from 1060 to 1089 K.[15,29,30,39,60,61] In Ref. 33, a value of 1060 K was used. However, in this work, we consider that 1082 K is a more reliable value because it has obtained by different simulation methods.[39] Therefore, we repeat the calculations performed in Ref. 33 using 1082 K instead of 1060 K. We have divided the calculations in 20 US windows, using the same order parameter to compute N as in Ref. 32 (and the same used in this work for the seeding technique). For each window, an NpT Monte Carlo simulation with bias potential $u_w = k(N - N_0)^2$ was performed (being k the bias constant 0.112 64 k_BT and N_0 the number of particles in the cluster around which the sampling window is centered). Our Monte Carlo simulations consisted of 5000 equilibration sweeps and 25 000 production sweeps. (Each sweep consisted of two MC cycles in which a particle trial move and a volume trial move are attempted.) The configuration obtained at the end of a sweep is compared with that at the beginning of the sweep and accepted or rejected according to the Metropolis criterion with the bias potential above mentioned. Our results are compared to those of Ref. 33 in Fig. 12.

From $\Delta G(N)$ in Fig. 12, we can obtain $\gamma_{cf}(N)$ as explained above (Fig. 13). For clusters larger than ~50 particles, the free energy reaches a plateau around 102 mJ/m^2. This value is very similar (about 3 mJ/m^2 higher) to that obtained in Ref. 33, so we can conclude that the effect of changing by about 20 K the melting temperature is very small.

With the seeding technique, we concluded that, within the accuracy of our data, γ_{cf} did not depend on temperature (see Fig. 9). Since the interfacial entropy is minus the derivative of γ_{cf} with respect to T, we concluded that the interfacial entropy was either zero or very small. We can double-check this statement by analysing our umbrella sampling data. By

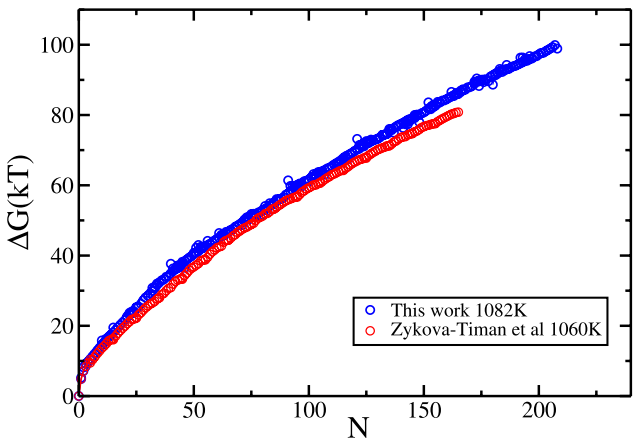

FIG. 12. Free energy barriers (ΔG) as a function of N at coexistence (blue circles) and at 1060 K (red circles), the latter from Ref. 33.

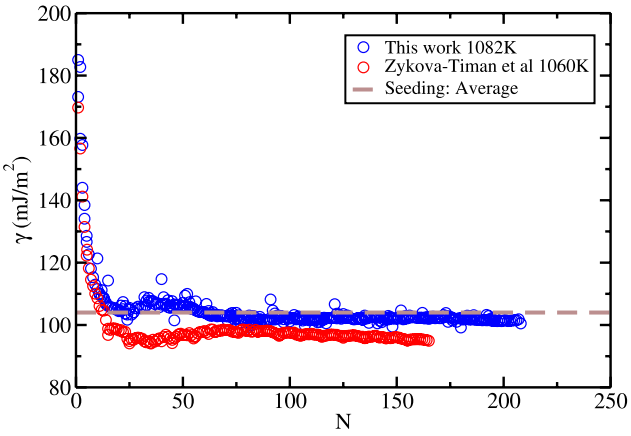

FIG. 13. Circles: Interfacial free energy as a function of the cluster size obtained from the free energy barriers shown in Fig. 12. Dashed line: average value from seeding simulations.

measuring the enthalpy of the system for each cluster size and subtracting the enthalpy of the liquid, we obtain the enthalpy of cluster formation as a function of the cluster size N. Then, we subtract $N\Delta H_m$ to such enthalpy and divide by the cluster's surface area (assuming a spherical shape) to obtain the interfacial enthalpy H_{cf}. The interfacial entropy, S_{cf}, is finally obtained as $S = (H_{cf} - \gamma)/T$. In Fig. 14, we plot the interfacial free energy and the two terms that add up to it (H_{cf} and $-TS_{cf}$) as a function of the cluster size.

As the cluster becomes larger, it is clear that γ_{cf} becomes increasingly dominated by the enthalpic term. For the largest simulated cluster (containing 210 particles) about 90% of the interfacial free energy is enthalpic. For such cluster size, the interfacial entropy is $S_{cf} = 0.01$ mJ/m^2 K, so small that it would lead to a decrease of γ of only 3 mJ/m^2 for a supercooling of 300 K. Such decrease is smaller than our error bar in the seeding method. From Fig. 14, it seems that for large clusters convergence will be reached for $H_{cf} \simeq \gamma$ and $S_{cf} \simeq 0$. The fact that γ_{cf} for NaCl is mainly enthalpic cannot be generalized to all systems. For instance, in water, the cost to create the ice-fluid interface seems to be entropic rather than enthalpic.[62] To conclude, the analysis performed from our umbrella sampling simulations confirms the conclusion drawn

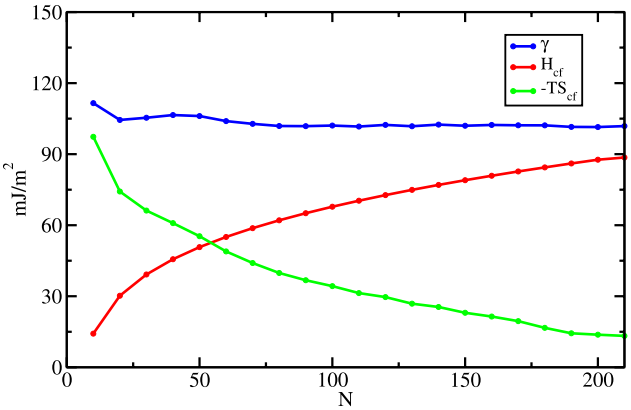

FIG. 14. Interfacial free energy (blue), interfacial enthalpy (red), and interfacial entropy multiplied by − T (green) as a function of the cluster size N.

from the seeding technique that γ_{cf} is either independent of T or varies very smoothly with it.

VII. DISCUSSION

The orientationaly averaged γ_{cf} obtained through the three different methodologies used in this work is about 100 mJ/m^2. This value is consistent with that obtained in Ref. 32 assuming a spherical cluster shape. The value is also similar, although about 10% higher, to that recently obtained by means of an analysis of capillary wave fluctuations of the crystal-melt interface.[48] In order to get a good agreement between the γ_{cf} calculated for a planar interface (via MI or Capillary Fluctuations[48]) and that obtained from crystal clusters (seeding and US), we did not need to resort to corrections[63] to the simplest version of CNT. The value of 100 mN/m for γ_{cf} clashes with the 36 mN/m obtained in Refs. 14 and 31. We suspect that the discrepancy may stem from finite size effects such as the comparable weight of surface and line tensions, arising when calculating contact angles with small droplets.[64] The good agreement between our results and those of Ref. 32 suggests that there are no irreducible size effects in the calculation of γ_{cf} using small NaCl crystal clusters.[33]

The MI method gives γ_{cf} for different crystal orientations, whereas both seeding and US only provide an orientationaly averaged γ_{cf}. Moreover, both seeding and US are subject to an assumption on the cluster shape and to an order parameter that arbitrarily provides a value for the number of particles in the crystal cluster. The MI method does not have these drawbacks, but in principle only allows to obtain a γ_{cf} at coexistence. In order to get the dependence of γ_{cf} with temperature, seeding is the best option. US is in principle also valid for that purpose, but it is computationally very expensive to compute free energy barriers at low supercoolings, where the critical clusters contain thousands of particles. For NaCl, we find that γ_{cf} does not depend on temperature (at constant pressure). This is not a general rule for all substances. For instance, recent studies for water show that γ_{cf} decreases when the temperature decreases.[18,28,62,65] Moreover, the seeding method permits the estimate of the nucleation rate as a function of temperature through the calculation of the attachment rate of particles to the critical cluster. The results are shown in Fig. 11(b) in purple squares and can be fitted using CNT (purple line in the same figure). The fit shows a good agreement with experimental data.[34–36] We have also used CNT to obtain a nucleation rate curve for US and MI. Since γ_{cf} does not depend on temperature, one can take the average γ_{cf} calculated at coexistence with these techniques and use CNT as we did to fit the seeding data to obtain the cyan curve shown in Fig. 11. Both US and MI give the same curve because they yield the same average γ_{cf}. Of course, the curve is very close to that obtained with seeding because all methods give very similar γ_{cf} (and γ_{cf} does not depend on T). Obtaining a nucleation curve from MI or US at coexistence can only be attempted if γ_{cf} does not depend on T (which, according to the seeding data shown in Fig. 9, seems to be the case for NaCl).

In the seeding section of the paper, we show that the shape of crystal clusters is spherical. Consequently, we have used the CNT expressions for a spherical cluster throughout

the paper. With such expressions, seeding and US give the same result as the MI method. The latter method, as opposed to the other two, does not depend on any assumption on the cluster's shape. Therefore, both our shape analysis and the consistency of all techniques when clusters are assumed to be spherical indicate that NaCl clusters are indeed spherical. This result appears in principle contradictory with that of Ref. 32 where the clusters were reported to be cubic. In Ref. 32, the typical critical cluster size was of the order of 100 ions. In Fig. 8(c), we show a cluster of nearly 100 particles that has been obtained by taking the particles inside a sphere from the bulk crystal lattice. The cluster is cubic rather than spherical, which means that when dealing with such small NaCl clusters, one cannot see anything else than cubic clusters due to the impossibility of obtaining a spherical shape with a few nodes of a cubic lattice.

The kinetic prefactor for the nucleation rate of NaCl is of the order of 10^{40} m^{-3} s^{-1}. This is about three orders of magnitude higher than that of realistic models of water (of the TIP4P family[66]) and of the same order of magnitude than that of the coarse-grain water model mW,[67] for which water is seen like a single atom.[18,28] This suggests that the orientational degrees of freedom of water slow down by a factor of 1000 the attachment of particles to the critical cluster with respect to atomic systems.

VIII. CONCLUSIONS

The orientationaly averaged interfacial free energy of NaCl evaluated via three independent techniques is $\gamma_{cf} = 100 \pm 5$ mJ/m^2. All methods consistently give this result, which is in good agreement with Ref. 32. The techniques employed have been the mold integration method, that provides γ_{cf} for different crystal orientations, and the seeding, and the umbrella sampling methods, that give an orientationaly averaged γ_{cf}. All studied orientations have a very similar γ_{cf} of around 100 mJ/m^2, except the (111) plane, whose γ_{cf} is 114 ± 1 mJ/m^2. The seeding method also allows estimating γ_{cf} for different temperatures. We find that, within the accuracy of our calculations, γ_{cf} does not depend on temperature. Consistently, our umbrella sampling data at coexistence show that the work needed to form the crystal-fluid interface is mainly enthalpic rather than entropic.

An analysis of the shape of crystal clusters in the supercooled fluid reveals that these have a spherical shape. Small clusters—containing about 100 particles—look cubic simply because it is not possible to obtain a sphere with few nodes of a cubic lattice.

The seeding method also allows estimating free energy barriers and nucleation rates for several temperatures. Using classical nucleation theory, we obtain a fit for our nucleation rate data that are consistent with experiments[34–36] and that extrapolate well to high supercoolings, where we have evaluated the rate with brute force simulations.

ACKNOWLEDGMENTS

All authors acknowledge the Spanish Ministry of Economy and Competitiveness for the financial support through the Project No. FIS2013-43209-P and the RES for providing supercomputing facilities (Project No. QCM-2015-1-0028). E. Sanz and J. R. Espinosa acknowledge financial support from the EU Grant No. 322326-COSAAC-FP7-PEOPLE-2012-CIG. E. Sanz and C. Valeriani from a Spanish tenure track Ramon y Cajal. E. Sanz thanks useful discussions with L. G. MacDowell and J. Benet.

[1]W. Boettinger, S. Coriell, A. Greer, A. Karma, W. Kurz, M. Rappaz, and R. Trivedi, Acta Mater. **48**, 43 (2000).
[2]D. P. Woodruff, *The Solid–Liquid Interface* (Cambridge University Press, Cambridge, 1973).
[3]K. F. Kelton, in *Crystal Nucleation in Liquids and Glasses* (Academic Press, Boston, 1991), Vol. 45, p. 75.
[4]K. F. Kelton, *Solid State Physics* (Academic Press, Dordrecht, 1991).
[5]M. Volmer and A. Weber, Z. Phys. Chem. **119**, 277 (1926).
[6]R. Becker and W. Doring, Ann. Phys. **24**, 719 (1935).
[7]L. Farkas, Z. Chem. Phys. **125**, 236 (1927).
[8]J. W. Gibbs, in *The Scientific Papers of J. Willard Gibbs* (Dover, 1961), Vol. 125.
[9]J. Q. Broughton and G. H. Gilmer, J. Chem. Phys. **84**, 5759 (1986).
[10]J. J. Hoyt, M. Asta, and A. Karma, Phys. Rev. Lett. **86**, 5530 (2001).
[11]A. Laio and M. Parrinello, Proc. Natl. Acad. Sci. U. S. A. **99**, 12562 (2002).
[12]S. Angioletti-Uberti, M. Ceriotti, P. D. Lee, and M. W. Finnis, Phys. Rev. B **81**, 125416 (2010).
[13]L. A. Fernandez, V. Martin-Mayor, B. Seoane, and P. Verrocchio, Phys. Rev. Lett. **108**, 165701 (2012).
[14]T. Zykova-Timan, D. Ceresoli, U. Tartaglino, and E. Tosatti, Phys. Rev. Lett. **94**, 176105 (2005).
[15]T. Zykova-Timan, D. Ceresoli, U. Tartaglino, and E. Tosatti, J. Chem. Phys. **125**, 164701 (2005).
[16]X. M. Bai and M. Li, J. Chem. Phys. **123**, 151102 (2005).
[17]B. C. Knott, V. Molinero, M. F. Doherty, and B. Peters, J. Am. Chem. Soc. **134**, 19544 (2012).
[18]E. Sanz, C. Vega, J. R. Espinosa, R. Caballero-Bernal, J. L. F. Abascal, and C. Valeriani, J. Am. Chem. Soc. **135**, 15008 (2013).
[19]S. Auer and D. Frenkel, Nature **409**, 1020 (2001).
[20]J. R. Espinosa, C. Vega, and E. Sanz, J. Chem. Phys. **141**, 134709 (2014).
[21]R. L. Davidchack and B. B. Laird, J. Chem. Phys. **118**, 7651 (2003).
[22]R. Benjamin and J. Horbach, J. Chem. Phys. **141**, 044715 (2014).
[23]R. L. Davidchack, J. Chem. Phys. **133**, 234701 (2010).
[24]Y. Mu and X. Song, Phys. Rev. E **74**, 031611 (2006).
[25]R. L. Davidchack, J. R. Morris, and B. B. Laird, J. Chem. Phys. **125**, 094710 (2006).
[26]R. Handel, R. L. Davidchack, J. Anwar, and A. Brukhno, Phys. Rev. Lett. **100**, 036104 (2008).
[27]R. L. Davidchack, R. Handel, J. Anwar, and A. V. Brukhno, J. Chem. Theory Comput. **8**, 2383 (2012).
[28]J. R. Espinosa, E. Sanz, C. Valeriani, and C. Vega, J. Chem. Phys. **141**, 18C529 (2014).
[29]F. Fumi and M. Tosi, J. Phys. Chem. Solids **25**, 31 (1964).
[30]M. Tosi and F. Fumi, J. Phys. Chem. Solids **25**, 45 (1964).
[31]T. Zykova-Timan, D. Ceresoli, U. Tartaglino, and E. Tosatti, J. Chem. Phys. **123**, 164701 (2005).
[32]C. Valeriani, E. Sanz, and D. Frenkel, J. Chem. Phys. **122**, 194501 (2005).
[33]T. Zykova-Timan, C. Valeriani, E. Sanz, D. Frenkel, and E. Tosatti, Phys. Rev. Lett. **100**, 036103 (2008).
[34]E. R. Buckle and A. R. Ubbelohde, Proc. R. Soc. London, Ser. A **259**, 325 (1960).
[35]E. R. Buckle, Proc. R. Soc. London, Ser. A **261**, 189 (1961).
[36]E. R. Buckle and A. R. Ubbelohde, Proc. R. Soc. London, Ser. A **261**, 197 (1961).
[37]L. Dang and D. E. Smith, J. Chem. Phys. **99**, 6950 (1993).
[38]I. S. Joung and T. E. Cheatham, J. Phys. Chem. B **112**, 9020 (2008).
[39]J. L. Aragones, E. Sanz, C. Valeriani, and C. Vega, J. Chem. Phys. **137**, 104507 (2012).
[40]U. Essmann, L. Perera, M. L. Berkowitz, T. Darden, H. Lee, and L. G. Pedersen, J. Chem. Phys. **103**, 8577 (1995).
[41]H. Berendsen, D. van der Spoel, and R. van Drunen, Comput. Phys. Commun. **91**, 43 (1995).
[42]B. Hess, C. Kutzner, D. van der Spoel, and E. Lindahl, J. Chem. Theory Comput. **4**, 435 (2008).
[43]G. Bussi, D. Donadio, and M. Parrinello, J. Chem. Phys. **126**, 014101 (2007).

[44]M. Parrinello and A. Rahman, J. Appl. Phys. **52**, 7182 (1981).
[45]T. Schilling and F. Schmid, J. Chem. Phys. **131**, 231102 (2009).
[46]J. R. Espinosa, E. Sanz, C. Valeriani, and C. Vega, J. Chem. Phys. **139**, 144502 (2013).
[47]P. W. Tasker, J. Phys. C: Solid State Phys. **12**, 4977 (1979).
[48]J. Benet, L. G. MacDowell, and E. Sanz, J. Chem. Phys. **142**, 134706 (2015).
[49]X. M. Bai and M. Li, J. Chem. Phys. **124**, 124707 (2006).
[50]R. G. Pereyra, I. Szleifer, and M. A. Carignano, J. Chem. Phys. **135**, 034508 (2011).
[51]S. Auer and D. Frenkel, J. Chem. Phys. **120**, 3015 (2004).
[52]P. R. ten Wolde, M. J. Ruiz-Montero, and D. Frenkel, J. Chem. Phys. **104**, 9932 (1996).
[53]P. R. ten Wolde, M. J. Ruiz-Montero, and D. Frenkel, Phys. Rev. Lett. **75**, 2714 (1995).
[54]D. Turnbull, J. Appl. Phys. **21**, 1022 (1950).
[55]R. S. Aga, J. R. Morris, J. J. Hoyt, and M. Mendelev, Phys. Rev. Lett. **96**, 245701 (2006).
[56]L. J. Peng, J. R. Morris, and R. S. Aga, J. Chem. Phys. **133**, 084505 (2010).
[57]G. M. Torrie and J. P. Valleau, J. Comput. Phys. **23**, 187 (1977).
[58]P. R. ten Wolde and D. Frenkel, J. Chem. Phys. **109**, 9901 (1998).
[59]A. Cacciuto, S. Auer, and D. Frenkel, J. Chem. Phys. **119**, 7467 (2003).
[60]J. Rowlinson and B. Widom, *Molecular Theory of Capillarity*, Dover Books on Chemistry (Dover Publications, 2002).
[61]J. Anwar, D. Frenkel, and M. G. Noro, J. Chem. Phys. **118**, 728 (2003).
[62]A. Reinhardt and J. P. K. Doye, J. Chem. Phys. **139**, 096102 (2013).
[63]S. Prestipino, A. Laio, and E. Tosatti, Phys. Rev. Lett. **108**, 225701 (2012).
[64]L. G. MacDowell, M. Müller, and K. Binder, Colloids Surf., A **206**, 277 (2002).
[65]L. Ickes, A. Welti, C. Hoose, and U. Lohmann, Phys. Chem. Chem. Phys. **17**, 5514 (2015).
[66]W. L. Jorgensen, J. Chandrasekhar, J. D. Madura, R. W. Impey, and M. L. Klein, J. Chem. Phys. **79**, 926 (1983).
[67]V. Molinero and E. B. Moore, J. Phys. Chem. B **113**, 4008 (2009).